JACS
JOURNAL OF THE AMERICAN CHEMICAL SOCIETY

Article

DOTA-Branched Organic Frameworks as Giant and Potent Metal Chelators

Chengjie Sun, Hongyu Lin, Xuanqing Gong, Zhaoxuan Yang, Yan Mo, Xiaoyuan Chen, and Jinhao Gao

J. Am. Chem. Soc., **Just Accepted Manuscript** • DOI: 10.1021/jacs.9b09269 • Publication Date (Web): 11 Dec 2019

Just Accepted

is published by the American Chemical Society. 1155 Sixteenth Street N.W., Washington, DC 20036

DOTA-Branched Organic Frameworks as Giant and Potent Metal Chelators

Chengjie Sun,[†,#] Hongyu Lin,[†,#] Xuanqing Gong,[†] Zhaoxuan Yang,[†] Yan Mo,[†] Xiaoyuan Chen,[‡] and Jinhao Gao*[,†]

[†]State Key Laboratory of Physical Chemistry of Solid Surfaces, The MOE Laboratory of Spectrochemical Analysis &Instrumentation, The Key Laboratory for Chemical Biology of Fujian Province, and Department of Chemical Biology, College of Chemistry and Chemical Engineering, Xiamen University, Xiamen 361005, China

[‡]Laboratory of Molecular Imaging and Nanomedicine, National Institute of Biomedical Imaging and Bioengineering, National Institutes of Health, Bethesda, MD 20892, United States

ABSTRACT: Multinuclear complexes as metallo-agents for clinical use have caught extensive attention. In this paper, using DOTA as both a functioning unit and a constructing junction, we build a series of DOTA-branched organic frameworks (**DBOF**) with multiple chelating holes by organizing DOTA layer by layer. These giant chelators are well characterized, which reveals their nano-sized and soft structures. Further experiments demonstrate that they could efficiently hold abundant metal ions with much higher kinetic stabilities than the conventional small DOTA chelator. Their corresponding polynuclear complexes containing Gd^{3+}, Tb^{3+}, or both show superior imaging properties, excellent feasibility for peripheral modification, and unusual kinetic stability. This work can be easily extended to the fabrication of diverse homo-multinuclear complexes and core/shell hetero-multinuclear complexes with multifunctional properties. We expect that this new type of giant molecules and the ligand-branching strategy would open up a new avenue for the design and construction of next-generation polymetallic agents with high performance and stabilities for biomedical applications.

INTRODUCTION

Metal ion-based agents play an indispensable role in biomedicine. Paramagnetic metal ions including Gd^{3+}, Mn^{2+}, and Fe^{3+} reside in the core of contrast agents for magnetic resonance imaging (MRI).[1] Radioactive metal isotopes, such as $^{90}Y^{3+}$, $^{111}In^{3+}$, $^{177}Lu^{3+}$, and $^{64}Cu^{2+}$, have been widely used in clinic for single-photon emission computerized tomography (SPECT)/positron-emission tomography (PET) and radiation therapy.[2] In addition, some metal ions own unique therapeutic effects for certain diseases, such as Pt^{2+} in cisplatin for cancers[3] and Bi^{3+} for *Helicobacter pylori*-related gastrointestinal disorders.[4] However, most of these functional metal ions are either toxic or not stable in the body.[5] A simple way to overcome these restrictions is to form safe and stable complexes with chelators for better biocompatibility and bioavailability.

Many efforts have been dedicated to the development of the chelators for these functional metal ions.[6-10] Diethylenetriamine pentaacetic acid (DTPA) and its derivatives (DTPAs) was attractive during the early days and frequently utilized for chelating these diagnostic or therapeutic metal ions. Unfortunately, the correlation between the use of Gd-DTPAs and the onset of nephrogenic systemic fibrosis (NSF) resulted in a "black box warning" from the U. S. Food and Drug Administration (FDA) and the cessation of their clinical use for chelating functional metal ions with relatively high toxicity.[1] Attention was then turned to 1,4,7,10-tetraazacyclododecane-1,4,7,10-tetraacetic acid (DOTA) and its derivatives (DOTAs) of better thermodynamic and kinetic stabilities.[11-15] In fact, gadolinium complexes of DOTAs (Gd-DOTA, Gd-HP-DO3A, and Gd-DO3A-butrol) have been very successful as MRI contrast agents in clinic.[1] Recently, ^{68}Ga-DOTA-TATE (NETSPOT®) and ^{177}Lu-DOTA-TATE (LUTATHERA®) have also been approved by the FDA as radiopharmaceuticals for PET and radiation therapy, respectively.[16]

Meanwhile, chelators with multiple holding sites for metal ions have caught extensive attention.[12, 17-22] They could form polymetallic complexes with appropriate metal ions, realizing synchronous delivery of multiple metal ions (either the same or different), which would significantly increase the efficiency and sensitivity of the agents, or achieve multifunctionalities.[1, 23-26] Besides, synergistic effects could be achieved through the cooperation among different metal centers within the same molecule. For example, multinuclear platinum complex BBR3464 has been shown to be superior over cisplatin and entered Phase II clinical trials.[27-29] In addition, this cooperation could also lead to new functions that cannot be accomplished by a single metal site or a simple mixture of metal complexes, which is demonstrated by the functioning of many metalloenzymes[30] and artificial enzymes developed based on them.[21, 31-33]

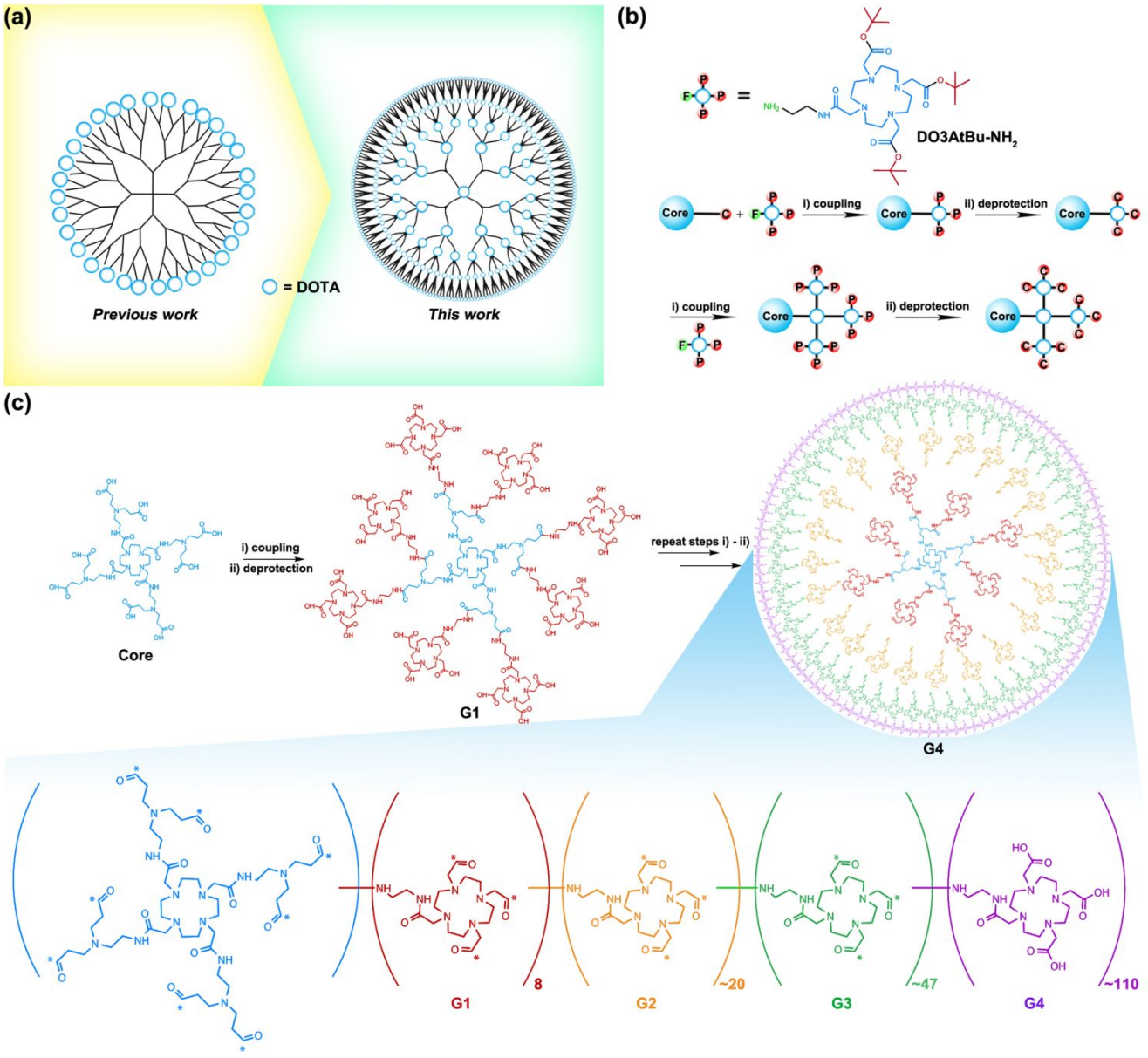

Figure 1. Structure of DOTA-branched organic frameworks. (a) Schematic illustration of the structure of DOTA-branched organic frameworks (**DBOF**), which is essentially different from traditional DOTA-modified dendrimers. (b) DO3A*t*Bu-NH_2 could be used as a protected building block to construct **DBOF** divergently. F = functional group (-NH_2), P = protective group (-*t*Bu), C = coupling group (-COOH). (c) Experimental fabrication of **DBOF**. i) Coupling: DO3A*t*Bu-NH_2, EDC·HCl, HOBT, DIPEA, DMF; ii) Deprotection: TFA, RT. * indicates the binding site for -NH- or -OH group.

Therefore, this type of chelators is appealing for the development of metallo-agents with higher efficiency, increased sensitivity, better biosafety and potential multifunctionality.

To further exploit the potential of polymetallic complexes for biomedical applications, we embarked on the search for unique chelating structures. Inspired by the distinctive structures of dendrimers and metal-organic frameworks (MOFs) that have been widely studied and utilized,[34-37] we herein designed a new type of frameworks ("giant chelators") with multiple chelating holes both in the interior and on the periphery (Figure 1a), which are single-molecular chelating structures with small-molecular ligands as the building blocks of the backbone. It is noted that this new giant molecular structure is completely different from the simple conjugates of traditional dendrimers and ligands in previous works.[38-39] To achieve the fabrication of such giant chelators, we developed a ligand-branching strategy that utilizes a small ligand as both the functioning unit and the constructing junction. In this work, DOTA was chosen as a ligand example to demonstrate the strategy explicitly. These DOTA-based giant chelators, named DOTA-branched organic frameworks (**DBOF**), could be assembled divergently from a central molecule derived from DOTA with repeating attachments of 2-aminoethyl-monoamide-DOTA-tris(*t*-Bu ester) (DO3A*t*Bu-NH_2) molecules as

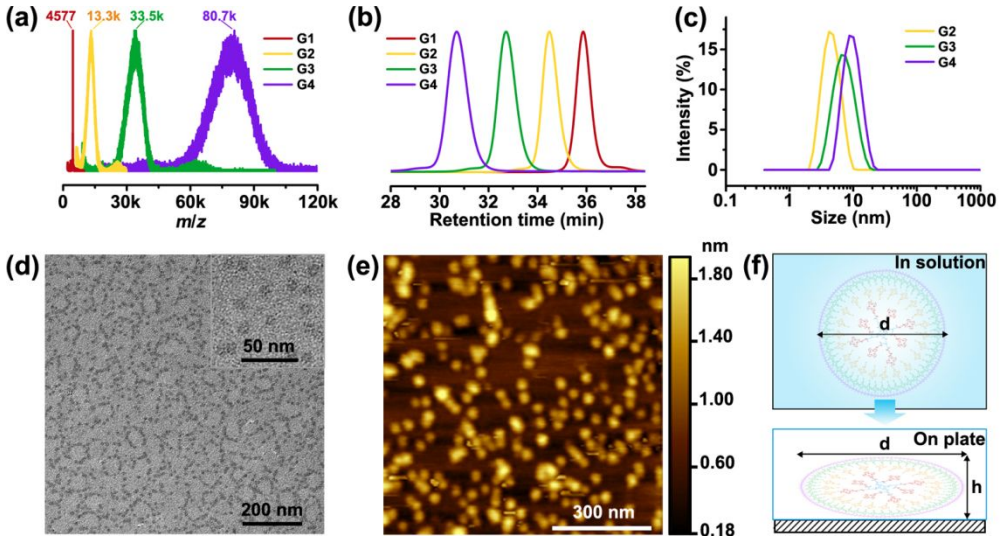

Figure 2. Characterization of **DBOF** giant chelators. (a) MALDI-TOF mass spectra of **G1**~**G4**. (b) GFC traces of **G1**~**G4**. (c) DLS intensity distributions of **G2**~**G4**. (d) Typical TEM images of **G4**. (e) An image of **G4** by atomic force microscopy. (f) Schematic illustration showing the deformation of **DBOF** on a plate.

protected junctions (Figure 1b). According to this strategy, we successfully synthesized **DBOF** with a series of generations. As expected, **DBOF** could efficiently chelate metal ions to form stable giant polymetallic complexes (**M-DBOF**). These **M-DBOF** complexes (*e.g.*, **Gd-DBOF** and **Tb-DBOF**) show superior imaging properties than their corresponding M-DOTA complexes. Besides, **DBOF** could be easily functionalized on the periphery (*e.g.*, PEGylation) because of abundant free carboxylic acid groups. More interestingly, **DBOF** can chelate with different metal ions to form hetero-multinuclear complexes with multifunctional properties. Furthermore, kinetic studies reveal that **M-DBOF** complexes are much more kinetically stable than M-DOTA complexes, which is extremely critical for *in vivo* applications. These **DBOF** giant chelators hold great potential as potent carriers for metal ions and would be enlightening for the development of next-generation metallo-agents for biomedical applications.

RESULTS AND DISCUSSION

Synthesis and characterizations of DBOF. Using DO3A*t*Bu-NH_2 as a protected branching junction, the strategy of which has not been reported before, **DBOF** could be rationally constructed based on an iterative strategy (Figure 1b). Through the efficient EDC-HOBt coupling (step i) and TFA deprotection (step ii) reactions, the DOTA-derived chelating holes could be packed layer by layer, maintaining the growth of **DBOF**. We chose a DOTA derivative that has eight carboxylic acid groups (Figure 1c, the structure in blue, and Scheme S1, Compound **5**) as the initial core to make the product after first construction cycle, **DBOF** Generation 1 (denoted as **G1**), large enough for dialysis, since purification by column chromatography could lead to considerable yield loss. Based on this strategy, we accomplished the synthesis of four generations, **G1**, **G2**, **G3**, and **G4**, without tedious column chromatography as detailed in Supporting Information.

The experimental chemical structures of **G1**~**G4** are shown in Figure 1c, which were characterized by mass spectrometry and nuclear magnetic resonance (NMR) spectroscopy (Figure S1-S17). Matrix-assisted laser desorption ionization time of flight mass spectrometry (MALDI-TOF-MS) results reveal the distributions of the molecular masses of **G2**~**G4** (Figure 2a), which is probably due to structural imperfections and/or molecular fragmentation by high laser power. The structural imperfections may arise from the strong steric congestion on the periphery of the macromolecules, and the fragmentation is inevitable since high laser power is necessary to ionize these macromolecules.[40] Therefore, the number of DOTA structures in each layer was estimated using the central molecular masses of the distributions. The numbers of the peripheral groups and DOTA chelating holes of **G1**~**G4** are summarized in Table S1. The gel filtration chromatography (GFC) results (Figure 2b) suggest that the size of the **DBOF** grows with the increase of generation as expected, whereas the size distribution in each generation remains narrow. The hydrodynamic diameters of the frameworks were 4.1nm (PdI: 0.117), 6.9 nm (PdI: 0.200), and 9.4 nm (PdI: 0.185) for **G2**, **G3**, and **G4**, respectively (Figure 2c). No credible result was obtained for **G1**, indicating that **G1** is too small to be measured by dynamic light scattering (DLS) analysis. To further visualize these giant chelators, **G4** was characterized by transmission electron microscopy (TEM) (Figure 2d) and atomic force microscopy (AFM) (Figure 2e). TEM shows that **G4** was uniformly circular with an average diameter of 11.6 nm, while AFM images shows that **G4** was elliptic on the mica plate with an average height of 1.29 nm and an average grain size of 15.70 nm. This oblate morphology revealed by TEM and AFM, which is different from the spherical morphology as indicated by DLS, is probably due to the symmetrical dendritic structure of the giant chelators that is soft, open, and deformable. This also accounts for the significantly larger particle size measured by AFM and TEM than the hydrodynamic diameter (Figure 2f). The observed particle size by AFM was slightly larger than that by TEM, which could be ascribed to the interaction between the tip of AFM and **G4**.[41] These results demonstrate that the size of the chelators reaches nanometers after a few synthesis

cycles. This would confer certain properties that are unique to nanomaterials

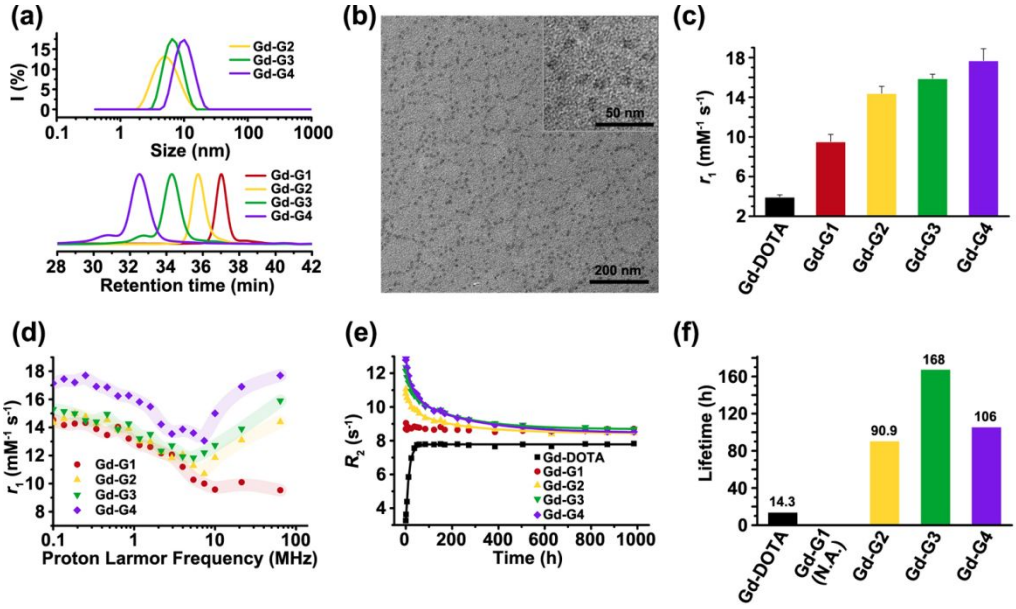

Figure 3. Characterization and properties of **Gd-DBOF** complexes. (a) DLS intensity distributions (top) and GFC (bottom) profiles of **Gd-DBOF**. (b) Typical TEM images of **Gd-G4**. (c) Comparison of r_1 values between **Gd-DBOF** and Gd-DOTA at 1.5 T. (d) Nuclear magnetic relaxation dispersion (NMRD) profiles of **Gd-DBOF** at 25 °C. (e) Changes on R_2 of 1 M HCl solutions containing the complexes at 25 °C over time. (f) The lifetimes of **Gd-DBOF** in 1 M HCl were significantly longer than that of Gd-DOTA. N.A., no available.

on the frameworks, such as high cellular uptake, long retention time, and controllable *in vivo* behaviors, which are highly desired for biomedical applications. [25]

Gd-DBOF complexes. We firstly employed these frameworks to chelate Gd^{3+} and investigated their characteristics in metal chelation and their performance in magnetic resonance imaging (MRI). MALDI-TOF-MS spectra of **Gd-G1** (Figure S18) demonstrate that nine metal ions were quantitatively coordinated by one **G1** molecule, which is consistent with the number of DOTA chelating holes in one **G1** molecule. The metal contents (Table S2) of **Gd-DBOF** complexes approached the metal content of the small Gd-DOTA complex, which are higher than those of most nanocarriers for metal ions, suggesting a considerable efficiency of **DBOF** in carrying metal ions.

DLS profiles (Figure 3a, top panel) reveal that the hydrodynamic diameters of **Gd-G2**~**G4** were 4.8 nm (PdI: 0.139), 6.4 nm (PdI: 0.075), and 9.5 nm (PdI: 0.094), respectively. Notably, only little change in either hydrodynamic diameter or size distribution was observed during chelation, indicating that metal ions were embedded into the ligands as expected. GFC profiles (Figure 3a, bottom panel) of **Gd-G1~G4** and TEM images (Figure 3b) of **Gd-G4** indicate that these giant chelates were spherical and monodispersed, which is inherited from **DBOF**. The average particle size of **Gd-G4** in TEM was 10.2 nm, which is slightly smaller than that of **G4** (11.6 nm), indicating that the structure of **Gd-G4** is more rigid than **G4**. These results indicate that **DBOF** acts like a umimolecular micelle customized for carrying hydrophilic metal complexes, which is hard to be accomplished by traditional umimolecular micelles since hydrophilic metal complexes are difficult to be physically enwrapped into the core of unimolecular micelles. Even that metal complexes could be chemically conjugated to the end groups of the core of the micelle, such conjugation is difficult to control and would restrict surface modifications and further affect the *in vivo* behaviors of the micelle.[38, 42] In contrast, the periphery of **M-DBOF** is open to various modifications and its *in vivo* behaviors are almost free of interference from hydrophilic metal complexes.

As Gd^{3+} is widely used in clinical MRI, we further studied the MRI-related properties of **Gd-DBOF**. The ionic longitudinal relaxivities (r_1) of **Gd-G1~G4** at 1.5 T were about 2.4-fold, 3.6-fold, 4.0-fold, and 4.5-fold higher than that of Gd-DOTA (Figure 3c), respectively. The high r_1 of **Gd-DBOF** should be ascribed to the longer rotational correlation times of the giant complexes, which was evidenced by the peak at 10-100 MHz in the nuclear magnetic relaxation dispersion (NMRD) profiles (Figure 3d).[43] The T_1-weighted phantom images of **Gd-DBOF** were significantly brighter than that of Gd-DOTA at a given Gd^{3+} concentration (Figure S20), which further demonstrates that **Gd-DBOF** could act as high-performance contrast agents for T_1-weighted MRI.

We further explored the chelating stability of **Gd-DBOF** by a classic relaxometric method.[44] It is well-known that small M-DOTAs complexes are highly kinetically stable, which could hardly be achieved by other forms of chelation.[45-47] Surprisingly, under highly acidic conditions (1 M HCl), much slower changes of proton transverse relaxation rates (R_2) were observed with **Gd-DBOF** than with Gd-DOTA (Figure 3e). Gd-DOTA was completely decomposed within 50 h, while the decompositions for **Gd-G2~G3** required more than 1000 h. Unfortunately, the decomposition of **Gd-G1** could not be evaluated by this method since the relaxivity of **Gd-G1** is similar to that of free Gd^{3+} ion under acidic

solutions. The exponential decay model was used to quantitatively evaluate the lifetimes of these complexes in the acidic solutions (detailed in the Supporting Information, Table S3), which are shown in Figure 3f. All **Gd-DBOF**

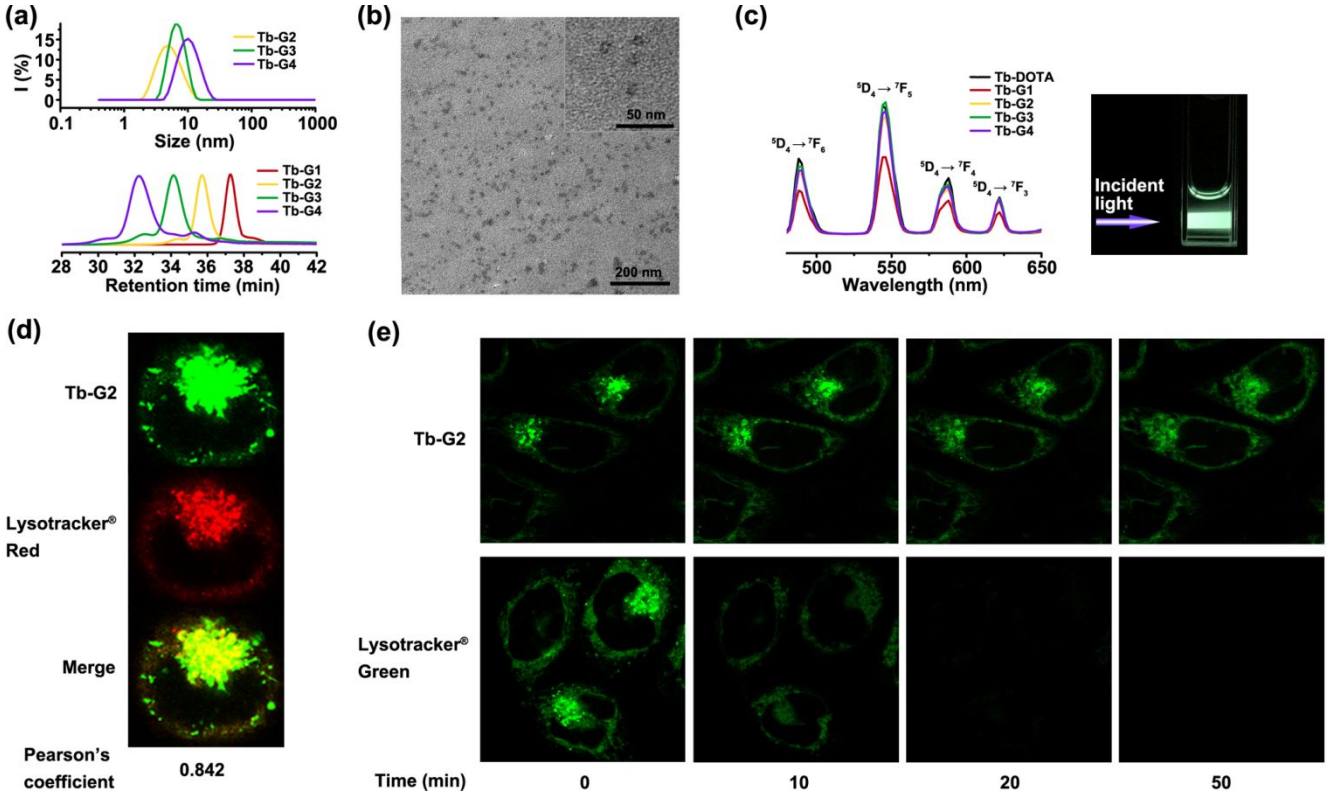

Figure 4. Tb-DBOF complexes for cell imaging. (a) DLS intensity distributions (top) and GFC (bottom) profiles of **Tb-DBOF**. (b) Typical TEM images of **Tb-G4**. (c) Emission spectra of **Tb-DBOF** and Tb-DOTA (left) and an optical photograph of the solution containing **Tb-G2** with exciting light (right). (d) Confocal microscopy images of HeLa cells after incubation with **Tb-G2** (top) and Lysotracker® Red (middle), the merged picture (bottom) reveals a significant degree of co-localization for both probes. (e) Comparison of photostabilities of **Tb-G2** and Lysotracker® Green in live HeLa cells.

(**Gd-G2~G4**) showed significantly longer lifetimes than Gd-DOTA. These results demonstrate that **Gd-DBOF** are much more kinetically stable than Gd-DOTA, which is crucial for biomedical applications.[46, 48]

Kinetic stability is one of the critical factors governing the design of metal-chelate-based agents, especially after the discovery of the relevance between the utilization of Gd^{3+} chelates and NSF.[49] Most of current approaches tackling the problem of kinetic stability are focusing on the structure optimization of small molecular ligands or simply attaching multiple small molecular ligands to the periphery of a certain polymeric backbone. For the first time, we established a macromolecular approach to fabricate giant chelators with multiple chelating ligands both in the interior and on the periphery of dendritic frameworks. Since these **DBOF** chelators are nanosized with dendritic structure, it is feasible to impart certain properties desired for biomedical applications, such as adjustable *in vivo* behaviors and lesion targeting, through size manipulation and post-construction functionalization.

Tb-DBOF complexes. To further demonstrate the versatility of **DBOF**, we prepared their Tb^{3+} complexes to study the fluorescence imaging properties. The results of DLS, GFC, and TEM characterizations of **Tb-DBOF** were similar to those of **Gd-DBOF** (Figure 4a-b). The emission fluorescence spectra of **Tb-DBOF** featured typical Tb^{3+}-based peaks, which originates from electron transitions between the $^5D_4$ state and the ^7F_j (j = 3~6) ground states (Figure 4c).[50] Tb^{3+} complexes are widely explored as fluorescence probes for cell imaging. However, most of the reported probes were small Tb complexes that are quickly excreted from cells.[51] In our study, after incubated with HeLa cells for 4 h, **Tb-G2~G4** could stay in the cells while **Tb-DOTA** and **Tb-G1** were cleared (Figure S21a).

Interestingly, **Tb-G2~G4** were found to localize in lysosomes. The degree of co-localization between the Tb^{3+} complexes and Lysotracker® Red was evaluated by the Pearson's coefficient (Figure S21b), which is larger than 0.6 for each of **Tb-G2~G4**, indicating their accumulation in lysosomes. Among them, **Tb-G2** had the highest co-localization degree (Figure 4d). It is well-known that lanthanide-based fluorescences are highly photostable,[52] therefore, we examined the photostability of **Tb-G2** in cells with Lysotracker® Green as a control. Upon continuous irradiation, the fluorescence of Lysotracker® Green faded away within 20 min, while the fluorescence of **Tb-G2** sustained even after 50 min (Figure 4e and Supplementary movie 1), which indicates that **Tb-G2** could stay in living cells for a relatively long time. **Tb-DBOF** complexes are promising potential fluorescence probes for long-time live cell imaging and lysosome tracking.

Gd-G4-PEG complex. DBOF not only have chelating holes in frameworks but also possess plentiful peripheral groups (carboxylic acid groups) for further modifications (Table

S1). To showcase this advantage, we modified **G4** with methoxylPEG1000-amine (marked as **G4-PEG**), which is widely used in biomedical applications.[53] The successful PEGylation of **G4** was evidenced by MALDI-TOF-MS, DLS,

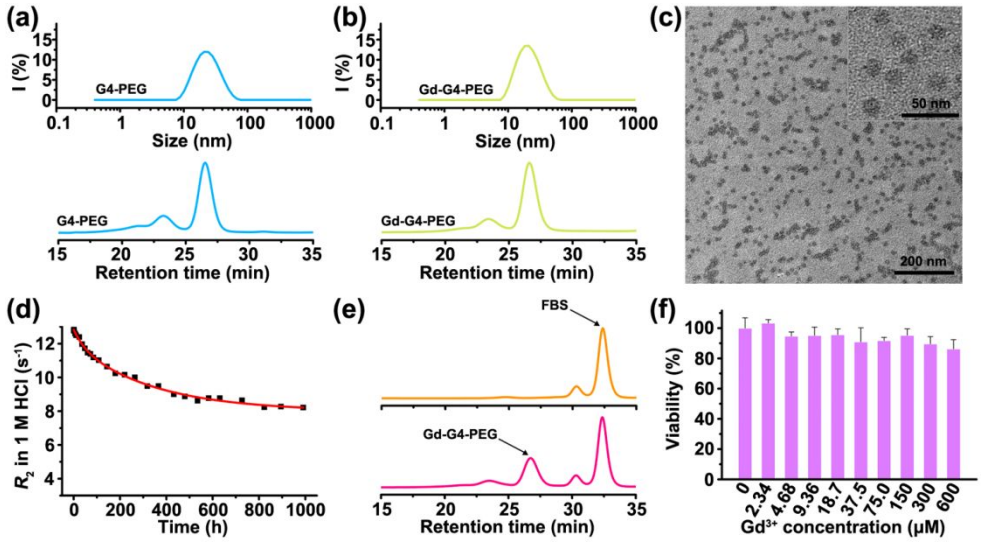

Figure 5. The PEGylation on the periphery of **DBOF** and **Gd-DBOF** complexes. (a) DLS intensity distributions (top) and GFC (bottom) profiles of **G4-PEG**. (b) DLS intensity distributions (top) and GFC (bottom) profiles of **Gd-G4-PEG**. (c) Typical TEM images of **Gd-G4-PEG**. (d) Changes on R_2 of 1 M HCl solution containing **Gd-G4-PEG** at 25 °C over time. (e) GFC profiles of FBS before (top) and after (bottom) incubated with **Gd-G4-PEG**. (f) MTT assays of HeLa cells incubated with **Gd-G4-PEG** for 24 h.

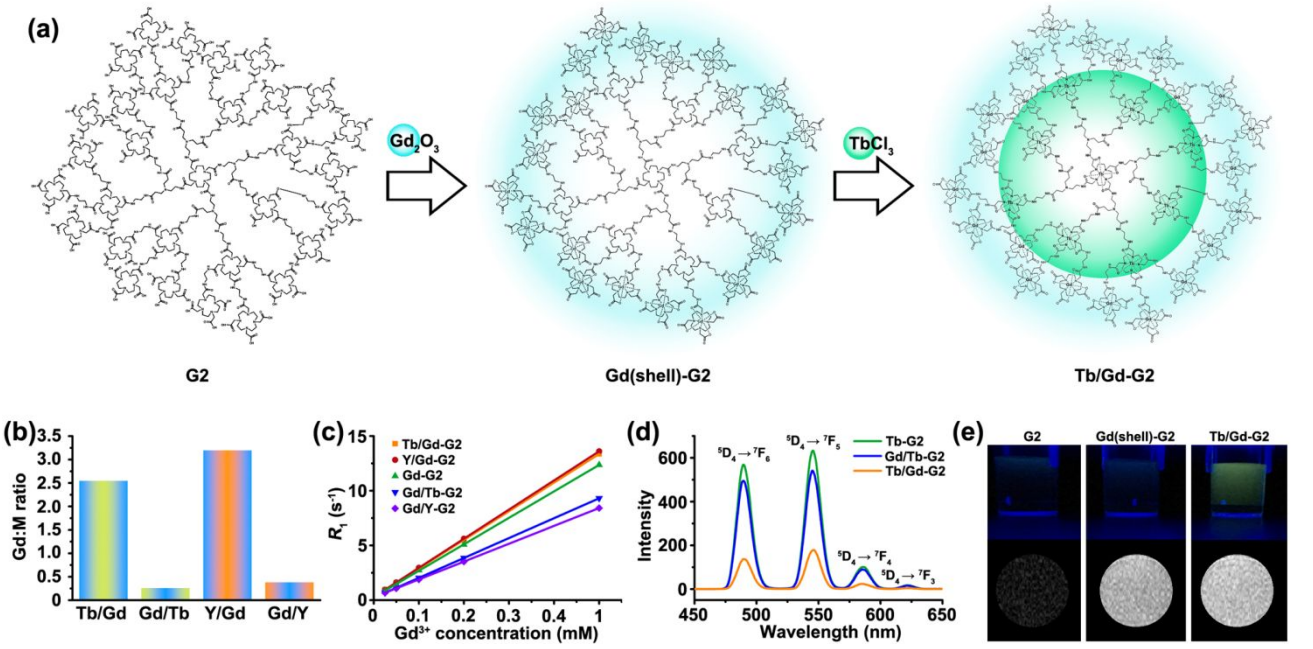

Figure 6. Facile formation of core/shell hetero-multinuclear complexes with multifunctional properties. (a) Using Gd_2O_3 as the source of Gd^{3+} and $TbCl_3$ as the source of Tb^{3+}, the **Tb/Gd-G2** core/shell complex was synthesized based on the difference in stability constant between the DOTA monoamide chelating holes in the shell and the DOTA tetraamide chelating holes in the core. (b) Molar Gd:M ratio of the core/shell complexes. (c) Relaxivity measurements of the core/shell complexes at 0.5 T, 25 ˚C. (d) Emission spectra of **Tb-G2**, **Gd/Tb-G2**, and **Tb/Gd-G2**, λ_{ex} = 254 nm. (e) Fluorescence images (top, λ_{ex} = 254 nm) and T_1 MRI phantom images (bottom) of **G2**, **Gd(shell)-G2**, and **Tb/Gd-G2** (0.5 T, 25 °C, TR = 100 ms, TE = 0.004 ms).

GFC, and TEM. The result of MALDI-TOF-MS (Figure S19) indicates that approximately 200 PEG chains were attached to **G4**, which has about 330 peripheral carboxylic acid groups. The hydrodynamic diameter increased from 9.4 nm (PdI: 0.185) to 22.3 nm (PdI: 0.216) after PEGylation (Figure 5a, top panel). Concomitantly, GFC profiles (Figure 5a, bottom panel) also reveal a significant change on retention time of the product (**G4**: 30.7 min, **G4-PEG**: 26.5 min), indicating a significant increase in particle size after PEGylation. None of retention time or hydrodynamic diameter changed during further chelation of **G4-PEG** with Gd^{3+} (marked as **Gd-G4-PEG**) (Figure 5b, hydrodynamic diameter: 19.5 nm, PdI: 0.159, retention time: 26.6 min), suggesting that Gd^{3+} were successfully implanted inside **G4-PEG**. TEM reveals that **Gd-G4-PEG** inherited the high monodispersity of **G4** with a size of 15.2 nm (Figure 5c).

Relaxivity measurents show that the r_1 value (8.7 mM^{-1} s^{-1}) of **Gd-G4-PEG** at 0.5 T was smaller than that of **Gd-G4** (15.0 mM^{-1} s^{-1}). This decrease in r_1 may be ascribed to the decrease in the water exchange rate of **Gd-G4-PEG**, which is caused by the amidation of the carboxylic acid groups in the shell of **G4** and the formation of the thick PEG shell. The exploration on kinetic stability further indicates that the R_2 change of **Gd-G4-PEG** (Figure 5d) was even slower than those of **Gd-DBOF** in 1 M HCl solution. The lifetime of **Gd-G4-PEG** was about 334 h, which is twenty-fold longer than that of Gd-DOTA. No significant change in relaxivity or hydrodynamic diameter was observed for **Gd-G4-PEG** and **Gd-G1~G4** during incubation in phosphate buffer saline (1 × PBS) at 37 ˚C for 2 weeks (Figure S22), indicating that these giant complexes are highly stable under physiological conditions.

The extremely high kinetic stability of **Gd-G4-PEG** offers great opportunities in fabrication of metallo-agents with high biosafety. To this end, we further evaluated the biocompatibility of **Gd-G4-PEG**. GFC analysis reveals few interactions of **Gd-G4-PEG** with serum proteins (Figure 5e), indicating no formation of protein corona on **Gd-G4-PEG**. Furthermore, MTT assays (Figure 5f) show that **Gd-G4-PEG** was of no apparent cytotoxicity even at up to 600 μM with respect to Gd^{3+}. Time dependent MRI of several organs and Gd biodistribution analysis (Figure S23) reveal that **Gd-G4-PEG** may have a favorable *in vivo* behavior for further applicaions in biomedical imaging. These preliminary results strongly indicate the promising potential of surface-engineered **DBOF** as metallo-agents with high biosafety and advanced properties.

M^2/M^1-G2 core/shell complex. Because of their multiplex nature, we explored the possibility of **DBOF** for heterometallic chelation to form hetero-multinuclear complexes with multifunctional properties. Using Gd_2O_3 as the source of Gd^{3+} ions and ethylenediaminetetraacetic acid (EDTA) to control the amount of Gd^{3+} ions, Gd(shell)-G2 could be constructed (Figure 6a), as demonstrated by the model reaction (Supporting Information S1.3, Figure S24, and Figure S25). By further Tb^{3+} chelation with Gd(shell)-G2, the fabrication of a **Tb/Gd-G2** core/shell complex could be accomplished (Figure 6a). Based on this protocol, **Gd/Tb-G2**, **Y/Gd-G2**, and **Gd/Y-G2** core/shell complexes could also be constructed. It is worth noting that during the chelating process, even that the metal reagents were used in large excess, the molar Gd:M ratios for **Tb/Gd-G2**, **Gd/Tb-G2**, **Y/Gd-G2**, and **Gd/Y-G2** were maintained at 2.6, 0.27, 3.2, and 0.40, respectively (Figure 6b), which is consistent with the ratio between the number of peripheral chelating holes and the number of interior chelating holes in **G2** (Table S1), indicating the achievement of the core/shell structure. Based on these core/shell complexes, we could further study the chelating property of **DBOF** selectively in the shell or in the core. Interestingly, the Tb^{3+} ions in the core have a larger q value (q = 1.43) than those in the shell (q = 0.90), and **Tb-G2** has a moderate q value (q = 0.99) consistent with the average of the q values of both the core and shell (Table S4). Furthermore, the complexes with Gd^{3+} in the shell (**Tb/Gd-G2** and **Y/Gd-G2**) have a much larger r_1 value (~13 mM^{-1} s^{-1}) than that (8 ~ 9 mM^{-1} s^{-1}) of the complexes with Gd^{3+} in the core (**Gd/Tb-G2** and **Gd/Y-G2**), while **Gd-G2** has an average level of r_1 value (12.1 mM^{-1} s^{-1}) (Figure 6c) (see Supporting Information S1.10 for details). The special properties found in these complexes demonstrate the achievement of the core/shell structure and reveal some of the distinct chelating characteristics of these giant chelators. The quantum yields (QYs) of the Tb complexes showed positive correlation with the number of Tb^{3+} ions per molecule (Figure 6d and Table S4), which could be attributed to the increased efficiency in energy transfer between Tb^{3+} ions and organic chromophores in the complexes.[54] As expected, **Tb/Gd-G2** and **Gd/Tb-G2** are capable of acting as dual-modal probes for both fluorescence imaging and contrast-enhanced MRI (Figure 6e and S26), indicating the enormous potential of **DBOF** as a platform for multimodal imaging. Further investigations are ongoing in our laboratory.

CONCLUSIONS

In conclusion, an innovative ligand-branching strategy has been successfully utilized to construct a series of DOTA-branched organic frameworks (**DBOF**) as giant chelators. These frameworks feature abundant interior and peripheral organized DOTA-derived chelating holes that could efficiently hold metal ions. The **M-DBOF** complexes are uniformly nanosized with high metal contents, which offer opportunities for the development of metallo-agents with high efficiency and sensitivity. Furthermore, the high kinetic stabilities of **M-DBOF** complexes also provide a potential solution for the stability problem of current metallo-agents. The versatility of **DBOF** in biomedical imaging are exemplified by Gd^{3+} or Tb^{3+} homometallic chelation, peripheral PEGlation, and Tb^{3+}/Gd^{3+} heterometallic chelation. The applications of **DBOF** could be easily extended to other metal-ion-based biomedical imaging, such as ^{64}Cu for PET and ^{99m}Tc for SPECT. More attractively, heterometallic **DBOF** complexes present a great opportunity for multimodal imaging. We believe that **DBOF** and their analogs will be emerging as a promising chelating platform for biomedicine, and the strategy behind the fabrication of these frameworks, the ligand-branching strategy, will be inspiring for the design and construction of novel giant molecules.

ASSOCIATED CONTENT

Supporting Information. The supporting information is available free of charge via the Internet at http://pubs.acs.org. Materials and details for synthesis and characterizations, NMR and mass spectra, MR images and fluorescence pictures, structure information (PDF).

AUTHOR INFORMATION

Corresponding Author

*jhgao@xmu.edu.cn

Author Contributions

#C.S. and H.L. contributed equally.

Notes

The authors declare no competing interest.

ACKNOWLEDGMENT

We thank Prof. B. Mao, Prof. J. Yan, and Y. Peng for the help in AFM test and data analysis. This work was supported by National Natural Science Foundation of China (21771148, 21602186, 21521004, and 81430041), IRT_17R66, the Natural Science Foundation of Fujian Province of China (2018J01011), and Fundamental Research Funds for the Central Universities (20720170020 and 20720180033).

REFERENCES

(1) Wahsner, J.; Gale, E. M.; Rodríguez-Rodríguez, A.; Caravan, P., Chemistry of MRI contrast agents: current challenges and new frontiers. *Chem. Rev.* **2019**, *119*, 957.

(2) Muthu, M. S.; Wilson, B., Multifunctional radionanomedicine: a novel nanoplatform for cancer imaging and therapy. *Nanomedicine* **2010**, *5*, 169.

(3) Kelland, L., The resurgence of platinum-based cancer chemotherapy. *Nat. Rev. Cancer* **2007**, *7*, 573.

(4) Mjos, K. D.; Orvig, C., Metallodrugs in medicinal inorganic chemistry. *Chem. Rev.* **2014**, *114*, 4540.

(5) Port, M.; Idée, J.-M.; Medina, C.; Robic, C.; Sabatou, M.; Corot, C., Efficiency, thermodynamic and kinetic stability of marketed gadolinium chelates and their possible clinical consequences: a critical review. *BioMetals* **2008**, *21*, 469.

(6) Lima, L. M.; Beyler, M.; Oukhatar, F.; Le Saec, P.; Faivre-Chauvet, A.; Platas-Iglesias, C.; Delgado, R.; Tripier, R., H_2Me-do2pa: an attractive chelator with fast, stable and inert $^{nat}Bi^{3+}$ and $^{213}Bi^{3+}$ complexation for potential a-radioimmunotherapy applications. *Chem. Commun.* **2014**, *50*, 12371.

(7) Vanasschen, C.; Molnar, E.; Tircso, G.; Kalman, F. K.; Toth, E.; Brandt, M.; Coenen, H. H.; Neumaier, B., Novel CDTA-based, bifunctional chelators for stable and inert Mn(II) complexation: synthesis and physicochemical characterization. *Inorg. Chem.* **2017**, *56*, 7746.

(8) Dai, L.; Jones, C. M.; Chan, W. T. K.; Pham, T. A.; Ling, X.; Gale, E. M.; Rotile, N. J.; Tai, W. C.; Anderson, C. J.; Caravan, P.; Law, G. L., Chiral DOTA chelators as an improved platform for biomedical imaging and therapy applications. *Nat. Commun.* **2018**, *9*, 857.

(9) Ma, L.; Wang, N.; Ma, R.; Li, C.; Xu, Z.; Tse, M. K.; Zhu, G., Monochalcoplatin: an actively transported, quickly reducible, and highly potent Pt^{IV} anticancer prodrug. *Angew. Chem. Int. Ed.* **2018**, *57*, 9098.

(10) Clough, T. J.; Jiang, L.; Wong, K. L.; Long, N. J., Ligand design strategies to increase stability of gadolinium-based magnetic resonance imaging contrast agents. *Nat. Commun.* **2019**, *10*, 1420.

(11) Stasiuk, G. J.; Long, N. J., The ubiquitous DOTA and its derivatives: the impact of 1,4,7,10-tetraazacyclododecane-1,4,7,10-tetraacetic acid on biomedical imaging. *Chem. Commun.* **2013**, *49*, 2732.

(12) Wang, L.; Zhu, X.; Tang, X.; Wu, C.; Zhou, Z.; Sun, C.; Deng, S.-L.; Ai, H.; Gao, J., A multiple gadolinium complex decorated fullerene as a highly sensitive T_1 contrast agent. *Chem. Commun.* **2015**, *51*, 4390.

(13) Wang, L.; Lin, H.; Ma, L.; Sun, C.; Huang, J.; Li, A.; Zhao, T.; Chen, Z.; Gao, J., Geometrical confinement directed albumin-based nanoprobes as enhanced T_1 contrast agents for tumor imaging. *J. Mater. Chem. B* **2017**, *5*, 8004.

(14) Wang, L.; Lin, H.; Chi, X.; Sun, C.; Huang, J.; Tang, X.; Chen, H.; Luo, X.; Yin, Z.; Gao, J., A self-assembled biocompatible nanoplatform for multimodal MR/fluorescence imaging assisted photothermal therapy and prognosis analysis. *Small* **2018**, *14*, 1801612.

(15) Yang, Z.; Lin, H.; Huang, J.; Li, A.; Sun, C.; Richmond, J.; Gao, J., A gadolinium-complex-based theranostic prodrug for in vivo tumour-targeted magnetic resonance imaging and therapy. *Chem. Commun.* **2019**, *55*, 4546.

(16) Long, N.; Wong, W.-T., *The chemistry of molecular imaging*. John Wiley & Sons Inc.: Hoboken, 2014.

(17) Mastarone, D. J.; Harrison, V. S.; Eckermann, A. L.; Parigi, G.; Luchinat, C.; Meade, T. J., A modular system for the synthesis of multiplexed magnetic resonance probes. *J. Am. Chem. Soc.* **2011**, *133*, 5329.

(18) Debroye, E.; Parac-Vogt, T. N., Towards polymetallic lanthanide complexes as dual contrast agents for magnetic resonance and optical imaging. *Chem. Soc. Rev.* **2014**, *43*, 8178.

(19) Lee, D. Y.; Kim, J. Y.; Lee, Y.; Lee, S.; Miao, W.; Kim, H. S.; Min, J. J.; Jon, S., Black pigment gallstone inspired platinum-chelated bilirubin nanoparticles for combined photoacoustic imaging and photothermal therapy of cancers. *Angew. Chem. Int. Ed.* **2017**, *56*, 13684.

(20) Shao, S.; Zhou, Q.; Si, J.; Tang, J.; Liu, X.; Wang, M.; Gao, J.; Wang, K.; Xu, R.; Shen, Y., A non-cytotoxic dendrimer with innate and potent anticancer and anti-metastatic activities. *Nat. Biomed. Eng.* **2017**, *1*, 745.

(21) Chen, J.; Wang, J.; Li, K.; Wang, Y.; Gruebele, M.; Ferguson, A. L.; Zimmerman, S. C., Polymeric "clickase" accelerates the copper click reaction of small molecules, proteins, and cells. *J. Am. Chem. Soc.* **2019**, *141*, 9693.

(22) Lan, G.; Ni, K.; Veroneau, S. S.; Feng, X.; Nash, G. T.; Luo, T.; Xu, Z.; Lin, W., Titanium-based nanoscale metal-organic framework for type I photodynamic therapy. *J. Am. Chem. Soc.* **2019**, *141*, 4204.

(23) Allen, T. M.; Cullis, P. R., Drug delivery systems: entering the mainstream. *Science* **2004**, *303*, 1818.

(24) Aime, S.; Castelli, D. D.; Crich, S. G.; Gianolio, E.; Terreno, E., Pushing the sensitivity envelope of lanthanide-based magnetic resonance imaging (MRI) contrast agents for molecular imaging applications. *Acc. Chem. Res.* **2009**, *42*, 822.

(25) Smith, B. R.; Gambhir, S. S., Nanomaterials for in vivo imaging. *Chem. Rev.* **2017**, *117*, 901.

(26) Sorensen, T. J.; Faulkner, S., Multimetallic lanthanide complexes: using kinetic control to define complex multimetallic arrays. *Acc. Chem. Res.* **2018**, *51*, 2493.

(27) Perego, P.; Caserini, C.; Gatti, L.; Carenini, N.; Romanelli, S.; Supino, R.; Colangelo, D.; Viano, I.; Leone, R.; Spinelli, S.; Pezzoni, G.; Manzotti, C.; Farrell, N.; Zunino, F., A novel trinuclear platinum complex overcomes cisplatin resistance in an osteosarcoma cell system. *Mol. Pharmacol.* **1999**, *55*, 528.

(28) Manzotti, C.; Pratesi, G.; Menta, E.; Di Domenico, R.; Cavalletti, E.; Fiebig, H. H.; Kelland, L. R.; Farrell, N.; Polizzi, D.; Supino, R.; Pezzoni, G.; Zunino, F., BBR 3464: a novel triplatinum complex, exhibiting a preclinical profile of antitumor efficacy different from cisplatin. *Clin. Cancer Res.* **2000**, *6*, 2626.

(29) Wheate, N., Multi-nuclear platinum complexes as anti-cancer drugs. *Coord. Chem. Rev.* **2003**, *241*, 133.

(30) Palermo, G.; Cavalli, A.; Klein, M. L.; Alfonso-Prieto, M.; Dal Peraro, M.; De Vivo, M., Catalytic metal ions and enzymatic processing of DNA and RNA. *Acc. Chem. Res.* **2015**, *48*, 220.

(31) Liu, C.; Wang, M.; Zhang, T.; Sun, H., DNA hydrolysis promoted by di- and multi-nuclear metal complexes. *Coord. Chem. Rev.* **2004**, *248*, 147.

(32) Artero, V.; Berggren, G.; Atta, M.; Caserta, G.; Roy, S.; Pecqueur, L.; Fontecave, M., From enzyme maturation to synthetic chemistry: the case of hydrogenases. *Acc. Chem. Res.* **2015**, *48*, 2380.

(33) Thanneeru, S.; Milazzo, N.; Lopes, A.; Wei, Z.; Angeles-Boza, A. M.; He, J., Synthetic polymers to promote cooperative Cu activity for O_2 activation: poly vs mono. *J. Am. Chem. Soc.* **2019**, *141*, 4252.

(34) Lee, C. C.; MacKay, J. A.; Frechet, J. M.; Szoka, F. C., Designing dendrimers for biological applications. *Nat. Biotechnol.* **2005**, *23*, 1517.

(35) Tomalia, D. A.; Khanna, S. N., A systematic framework and nanoperiodic concept for unifying nanoscience: hard/soft nanoelements, superatoms, meta-atoms, new emerging properties, periodic property patterns, and predictive mendeleev-like nanoperiodic tables. *Chem. Rev.* **2016**, *116*, 2705.

(36) Della Rocca, J.; Liu, D.; Lin, W., Nanoscale metal-organic frameworks for biomedical imaging and drug delivery. *Acc. Chem. Res.* **2011**, *44*, 957.

(37) Furukawa, H.; Cordova, K. E.; O'Keeffe, M.; Yaghi, O. M., The chemistry and applications of metal-organic frameworks. *Science* **2013**, *341*, 1230444.

(38) Margerum, L. D.; Campion, B. K.; Koo, M.; Shargill, N.; Lai, J.-J.; Marumoto, A.; Christian Sontum, P., Gadolinium(III) DO3A macrocycles and polyethylene glycol coupled to dendrimers effect of molecular weight on physical and biological properties of macromolecular magnetic resonance imaging contrast agents. *J. Alloys Compd.* **1997**, *249*, 185.

(39) Menjoge, A. R.; Kannan, R. M.; Tomalia, D. A., Dendrimer-based drug and imaging conjugates: design considerations for nanomedical applications. *Drug Discovery Today* **2010**, *15*, 171.

(40) Ficker, M.; Paolucci, V.; Christensen, J. B., Improved large-scale synthesis and characterization of small and medium generation PAMAM dendrimers. *Can. J. Chem.* **2017**, *95*, 954.

(41) Li, J.; Piehler, L. T.; Qin, D.; Baker, J. R.; Tomalia, D. A.; Meier, D. J., Visualization and characterization of poly(amidoamine) dendrimers by atomic force microscopy. *Langmuir* **2000**, *16*, 5613.

(42) Eetezadi, S.; Ekdawi, S. N.; Allen, C., The challenges facing block copolymer micelles for cancer therapy: in vivo barriers and clinical translation. *Adv. Drug Delivery Rev.* **2015**, *91*, 7.

(43) Caravan, P., Strategies for increasing the sensitivity of gadolinium based MRI contrast agents. *Chem. Soc. Rev.* **2006**, *35*, 512.

(44) Laurent, S.; Vander, L.; Copoix, F.; Muller, R. N., Stability of MRI paramagnetic contrast media: a proton relaxometric protocol for transmetalation assessment. *Invest. Radiol.* **2001**, *36*, 115.

(45) Pasha, A.; Tircso, G.; Benyo, E. T.; Brucher, E.; Sherry, A. D., Synthesis and characterization of DOTA-(amide)$_4$ derivatives: equilibrium and kinetic behavior of their lanthanide(III) complexes. *Eur. J. Inorg. Chem.* **2007**, *2007*, 4340.

(46) Drahos, B.; Lukes, I.; Toth, E., Manganese(II) complexes as potential contrast agents for MRI. *Eur. J. Inorg. Chem.* **2012**, *2012*, 1975.

(47) Woods, M.; Payne, K. M.; Valente, E. J.; Kucera, B. E.; Young, V. G., Jr., Crystal structures of DOTMA chelates from Ce^{3+} to Yb^{3+} : evidence for a continuum of metal ion hydration states. *Chem. - Eur. J.* **2019**, *25*, 9997.

(48) Huckle, J. E.; Altun, E.; Jay, M.; Semelka, R. C., Gadolinium deposition in humans: when did we learn that gadolinium was deposited in vivo? *Invest. Radiol.* **2016**, *51*, 236.

(49) Sherry, A. D.; Caravan, P.; Lenkinski, R. E., Primer on gadolinium chemistry. *J. Magn. Reson. Imaging* **2009**, *30*, 1240.

(50) Li, M.; Selvin, P. R., Luminescent polyaminocarboxylate chelates of terbium and europium: the effect of chelate structure. *J. Am. Chem. Soc.* **1995**, *117*, 8132.

(51) Coogan, M. P.; Fernandez-Moreira, V., Progress with, and prospects for, metal complexes in cell imaging. *Chem. Commun.* **2014**, *50*, 384.

(52) Kovacs, D.; Lu, X.; Meszaros, L. S.; Ott, M.; Andres, J.; Borbas, K. E., Photophysics of coumarin and carbostyril-sensitized luminescent lanthanide complexes: implications for complex design in multiplex detection. *J. Am. Chem. Soc.* **2017**, *139*, 5756.

(53) Knop, K.; Hoogenboom, R.; Fischer, D.; Schubert, U. S., Poly(ethylene glycol) in drug delivery: pros and cons as well as potential alternatives. *Angew. Chem. Int. Ed.* **2010**, *49*, 6288.

(54) Cross, J. P.; Lauz, M.; Badger, P. D.; Petoud, S., Polymetallic lanthanide complexes with PAMAM-naphthalimide dendritic ligands: luminescent lanthanide complexes formed in solution. *J. Am. Chem. Soc.* **2004**, *126*, 16278.

Table of contents (TOC)